2013 European Control Conference (ECC)
July 17-19, 2013, Zürich, Switzerland.

Rotational Start-up of Tethered Airplanes Based on Nonlinear MPC and MHE

Mario Zanon, Sébastien Gros and Moritz Diehl

Abstract— **The idea of Airborne Wind Energy (AWE) is to generate power by flying a tethered airfoil across the windflow. Tethered flight is a fast, strongly nonlinear, unstable and constrained process, motivating control approaches based on fast Nonlinear Model Predictive Control (NMPC) and state estimation approaches based on Moving Horizon Estimation (MHE). In particular, the start-up phase of AWE systems is an involved procedure, and starting and landing using NMPC has not been investigated yet. In this paper, a control strategy for starting-up AWE systems is proposed, based on a rotating carousel that is currently built at the KU Leuven. A computationally efficient 6-DOF control model for a small-scale, rigid airfoil is presented. We present and investigate a control scheme based on receding-horizon Nonlinear Model Predictive Control to track reference trajectories and Moving Horizon Estimation to estimate the actual system state and parameters. The MHE shceme is able to estimate also the wind speed, given no direct wind measurement.**

Keywords **: flight control, fast NMPC and MHE, trajectory tracking**

I. INTRODUCTION

Over the last years, conventional wind turbines have grown in size and mass up to a scale at which the major challenges are posed by the structural loads [1], [2]. The main idea behind Airborne Wind Energy (AWE) is to eliminate all the elements of the system which are not essential for power extraction, resulting in a much lighter structure that only involves an airfoil tethered to the ground. In this configuration, higher altitudes can be reached and the swept area is not fixed by the structure of the system, but can be optimized so as to maximise the extracted power. The system is thus free to operate in previously inaccessible portions of the wind field, where higher wind resources can be found. In the seminal paper [3], crosswind flight has been proposed as the most efficient method to extract power from the airmass. Having the airfoil flying at high velocity across the wind direction, two options have been proposed to extract the power. The first one is based on a pumping cycle divided in two phases, having the system a) reeling out the tether while the airfoil strongly pulls it and b) reeling in the tether while the airfoil flies back at low lift. The second option consists in flying at constant tether length using on-board turbines to generate power.

The potential of this technology has been established in theory [3], nevertheless many engineering questions still need to be addressed for a practical implementation. In the design of an AWE system, control issues are still a challenge that needs to be adequately addressed. The system needs to be operated in very different stages, including a) launch and retrieval, and b) power generation. The problem of control during power generation has been investigated in [4] and is the object of further research. This paper focuses on the problem of control during the launch and retrieval of the airfoil for a pumping-mode application.

The system dynamics are strongly nonlinear and actuator limitations as well as path constraints (e.g. the flight envelope) need to be satisfied by the controller. This paper proposes to tackle the control problem through Nonlinear Model Predictive Control (NMPC), which accounts for constraints and nonlinearities. The system dynamics are also strongly influenced by the wind speed and direction, which need to be known by the controller and can often not be measured reliably. Moving Horizon Estimation (MHE) features combined state and parameter estimation, allowing for online estimation of unmeasured parameters.

Both NMPC and MHE require to compute online the solution of an optimal control problem. When classical implementations of those techniques are applied to fast processes, two issues arise: a) the computational time can become too large to allow real time implementations, and b) the latency between the measurements and the application of the new control input can be excessively large, hence introducing significant delays in the system dynamics.

AWE systems exhibit fast, unstable and perturbed dynamics, thus the aforementioned issues become critical for the application of the NMPC and MHE scheme to a real system. The Real-Time Iteration (RTI) scheme [5], [6] addresses both issues by performing only a single Newton-type iteration per sampling instant, and making use of the initial value embedding. The initial value embedding allows to solve the problem efficiently, but also to prepare most of the computations before the initial state is known. Once the state estimate is available, the system has been already simulated and the sensitivities computed, thus the solution requires only few computations, resulting in a negligible latency.

In [4], [7] a fast NMPC controller based on the RTI scheme was successfully tested for the control of a tethered

M. Zanon, S. Gros and M. Diehl are with the Optimization in Engineering Center (OPTEC), K.U. Leuven, Kasteelpark Arenberg 10, B-3001 Leuven-Heverlee, Belgium. mario.zanon@esat.kuleuven.be

* This research was supported by Research Council KUL: PFV/10/002 Optimization in Engineering Center OPTEC, GOA/10/09 MaNet and GOA/10/11 Global real- time optimal control of autonomous robots and mechatronic systems. Flemish Government: IOF / KP / SCORES4CHEM, FWO: PhD/postdoc grants and projects: G.0320.08 (convex MPC), G.0377.09 (Mechatronics MPC); IWT: PhD Grants, projects: SBO LeCoPro; Belgian Federal Science Policy Office: IUAP P7 (DYSCO, Dynamical systems, control and optimization, 2012-2017); EU: FP7- EMBOCON (ICT-248940), FP7-SADCO (MC ITN-264735), ERC ST HIGHWIND (259 166), Eurostars SMART, ACCM.

airfoil for power generation in the presence of wind disturbances. In [8] sampling times of 1 ms were obtained with a simple model. The model considered the airfoil as a point-mass, assuming a) a perfect control of the time derivative of the lift coefficient C_{L}, b) a perfect control of the roll rate, c) that the side slip is perfectly cancelled by some ad-hoc control, and d) that the yaw rate is unbounded. Because these assumptions are not realistic in practice, a more elaborate control model is required.

In this paper a model is used, that considers the airfoil as a rigid-body, 6-DOF object interacting with the air mass. The full rotational dynamics are modeled and it is assumed that the aileron and elevator deflection rates are directly controlled. A control scheme based on MHE and NMPC using the proposed model and tracking a static reference is presented, resulting in a computational performance that is suitable for a real-time application. The problem of defining a reference trajectory that robustly satisfies the problem constraints is beyond the scope of this paper.

This paper is organized as follows. The process model is presented in Section II, the MHE and NMPC schemes are proposed in Section III. The control strategy for the launch and retrieval phases is detailed in Section IV. Simulation results are presented in Section V. Future developments and conclusions are proposed in Section VI.

Contribution of the paper: this paper proposes a control scheme for the rotational startup, based on an efficient formulation and implementation to allow for a real-time application. The MHE is formulated in order to estimate the wind speed and direction in the absence of direct measurements, thus increasing the robustness of the proposed scheme.

II. System Model

A. Plane Model

The airfoil is considered as a rigid body having 6 degrees of freedom (DOF). The position of the airfoil center of mass is described through a set of Cartesian coordinates $\{x,y,z\}$ relative to the rotating reference frame e_{T} , attached to the carousel arm tip. The reference frame E is attached to the plane, with the x-axis pointing to the nose of the plane, the y-axis aligned with the left wing and the z-axis defined so as to yield a right-handed orthonormal frame. The change of reference frame $E \to e_{\mathrm{T}}$ is obtained by the rotation matrix $R = [e_1\ e_2\ e_3]$. In this paper, a full parametrization of R is used, as already proposed in [9].

Let $P = [x\ y\ z]^T$, $P_{\mathrm{T}} = [r_{\mathrm{T}}\ 0\ 0]^T$, with r_{T} the arm length and R_δ the matrix defined by a vertical rotation of the carousel by an angle δ. Using $P_E = R_\delta (P + P_{\mathrm{T}})$, the kinetic and potential energy functions associated to the airfoil read:

$$\mathcal{T}_{\mathrm{A}} = \tfrac{1}{2} m_{\mathrm{A}} \dot{P}_E^T \dot{P}_E + \tfrac{1}{2} \omega^T J_A \omega, \quad \mathcal{V}_{\mathrm{A}} = m_{\mathrm{A}} g z,$$

The Lagrangian associated to the translational dynamics of the system reads:

$$\mathcal{L} = \mathcal{T}_{\mathrm{A}} - \mathcal{V}_{\mathrm{A}} + \mu c, \quad c = \frac{1}{2}\left(P^T P - r^2\right),$$

where r is the tether length. Note that the tether kinetic and potential energy has been neglected in this model.

As the carousel inertia is much bigger than the plane inertia, direct control of the second time derivative of $W = [r\ \ \delta]^T$ can be asssumed. The dynamics of the tethered plane are given by:

$$\begin{aligned}
&\mathcal{M}_0 \begin{bmatrix} \ddot{P} \\ \dot{\omega} \\ \mu \end{bmatrix} = G, \qquad G = \begin{bmatrix} F - \nabla_P \mathcal{V}_{\mathrm{A}} \\ T - \omega \times J_{\mathrm{A}} \omega \\ -\ddot{c}_0 \end{bmatrix}, \\
&\mathcal{M}_0 = \begin{bmatrix} mI_3 & 0 & \nabla_P c \\ 0 & J_{\mathrm{A}} & 0 \\ (\nabla_P c)^T & 0 & 0 \end{bmatrix}, \\
&\dot{R} = R\Omega - R_\delta \dot{R}_\delta R,
\end{aligned} \tag{1}$$

where F and T are respectively the aerodynamic forces and torques [10], which yield strong nonlinearities in the model equations. The angular velocity matrix Ω is given by $\Omega = \omega_\times$ and $\ddot{c}_0$ is given by:

$$\begin{aligned}
\dot{c} &= (\nabla_P c)^T \dot{P} + (\nabla_W c)^T \dot{W}, \\
\ddot{c} &= (\nabla_P \dot{c})^T \dot{P} + (\nabla_{\dot{P}} \dot{c})^T \ddot{P} + (\nabla_W \dot{c})^T \dot{W} + (\nabla_{\dot{W}} \dot{c})^T \ddot{W} \\
&= (\nabla_P c)^T \ddot{P} + \ddot{c}_0.
\end{aligned} \tag{2}$$

Because a Cartesian coordinate system is used, the generalized forces F in (1) are given by the sum of the aerodynamic forces acting at the airfoil center of mass, projected in frame e_{T}. Introducing the relative velocity v, i.e. the velocity of the airfoil w.r.t the air mass given by:

$$v = \left[\dot{x} - \dot{\delta} y, \dot{y} + \dot{\delta}(r_A + x), \dot{z}\right]^T - R_\delta^T w,$$

where $w = [w_x, w_y, 0]^T \in \mathcal{W} \subset \mathbb{R}^3$ is the wind velocity field. The norms of the lift and drag forces are given by [11]:

$$\|F_{\mathrm{L}}\| = \frac{1}{2}\rho C_{\mathrm{L}} \|v\|^2, \qquad \|F_{\mathrm{D}}\| = \frac{1}{2}\rho C_{\mathrm{D}} \|v\|^2,$$

where C_{L} and C_{D} are the lift and drag coefficient respectively, ρ is the air density and the airfoil surface A has been included in the coefficients C_{L} and C_{D}.

The lift force is orthogonal to the relative velocity v, moreover, it is assumed in this model that the lift force is orthogonal to the airfoil transversal axis spanned by E_y, therefore the lift force is collinear to the vector L given by:

$$L = v \times E_y.$$

Note that L is normed to $\|v\|$. The drag force is defined as collinear and opposed to the relative velocity v. The lift and drag forces, F_{L} and F_{D} acting on the airfoil are therefore

$$F_{\mathrm{L}} = \frac{1}{2}\rho C_{\mathrm{L}} \|v\| L, \qquad F_{\mathrm{D}} = -\frac{1}{2}\rho C_{\mathrm{D}} \|v\| v.$$

In order to compute the lift and drag forces in frame e_{T}, vectors E_y and v shall be projected in e_{T}. The resulting total aerodynamic force is:

$$F_{\mathrm{A}} = \frac{1}{2}\rho \left(C_{\mathrm{L}} [v]_{e_{\mathrm{T}}} \times e_2 - C_{\mathrm{D}} [v]_{e_{\mathrm{T}}}\right) \|v\|,$$

For the aerodynamic torques the following model is proposed [11]:

$$T_{\mathrm{A}} = \frac{1}{2}\rho\|v\|^2 \begin{bmatrix} S & 0 & 0 \\ 0 & C & 0 \\ 0 & 0 & S \end{bmatrix} \cdot \begin{bmatrix} C_{\mathrm{R}} \\ C_{\mathrm{P}} \\ C_{\mathrm{Y}} \end{bmatrix}, \quad (3)$$

where S is the wing span, C the wing chord. The lift, drag, roll, pitch and yaw coefficients, C_{L}, C_{D}, C_{R}, C_{P} and C_{Y} respectively, are given by [12]:

$$\begin{aligned} C_{\mathrm{L}} &= C_{\mathrm{L}}^{\alpha}\alpha + C_{\mathrm{L}}^{p}u_p + C_{\mathrm{L}}^{r}u_r + C_{\mathrm{L}}^{0}, \\ C_{\mathrm{D}} &= C_{\mathrm{D}}^{\alpha}\alpha + C_{\mathrm{D}}^{\alpha 2}\alpha^2 + C_{\mathrm{D}}^{\beta 2}\beta^2 + C_{\mathrm{D}}^{p}u_p + C_{\mathrm{D}}^{r}u_r + C_{\mathrm{D}}^{0}, \\ C_{\mathrm{R}} &= -R_{\mathrm{D}}\omega_{\mathrm{l}} + C_{\mathrm{R}}^{\beta}\beta_{\mathrm{T}} + C_{\mathrm{R}}^{\alpha\beta}\alpha_{\mathrm{T}}\beta_{\mathrm{T}} + C_{\mathrm{R}}^{r}u_r, \\ C_{\mathrm{P}} &= C_{\mathrm{P}}^{\alpha}\alpha_{\mathrm{T}} + C_{\mathrm{P}}^{p}u_p + C_{\mathrm{P}}^{r}u_r + C_{\mathrm{P}}^{0}, \\ C_{\mathrm{Y}} &= C_{\mathrm{Y}}^{\beta}\beta_{\mathrm{T}} + C_{\mathrm{Y}}^{\alpha\beta}\alpha_{\mathrm{T}}\beta_{\mathrm{T}}, \end{aligned} \quad (4)$$

where α is the aircraft angle of attack, α_{T} the tail angle of attack, and β_{T} the tail side-slip angle, and u_r, u_p are the ailerons and elevator deflection respectively. In this paper, we assume that the time derivatives of the deflections, $\dot{u}_r$ and $\dot{u}_p$, are directly controlled. The aerodynamic coefficients have been estimated for the small scale setup at KU Leuven through wind tunnel experiments and in-flight estimation [10]. The tail effective velocity v_{T} is:

$$v_{\mathrm{T}} = \omega \times \begin{bmatrix} -L_{\mathrm{T}} \\ 0 \\ 0 \end{bmatrix} + v, \quad (5)$$

where the parameter L_{T} stands for the tail effective length. The angles α, α_{T}, β and β_{T} are well approximated by:

$$\begin{aligned} \alpha &= -\frac{v^z}{v^x}, & \alpha_{\mathrm{T}} &= -\frac{v_{\mathrm{T}}^z}{v_{\mathrm{T}}^x}, \\ \beta &= \frac{v^y}{\sqrt{(v^x)^2 + (v^z)^2}}, & \beta_{\mathrm{T}} &= \frac{v_{\mathrm{T}}^y}{\sqrt{(v_{\mathrm{T}}^x)^2 + (v_{\mathrm{T}}^z)^2}}. \end{aligned} \quad (6)$$

In this paper the tether drag has been neglected. NMPC has been tested in simulations with this an accurate drag model, but the results have shown that the difference in the trajectories is negligible.

All model parameters can be found in [10]. In the following, the process dynamics and the process initial conditions will be put in the form:

$$\mathcal{M}(\mathcal{X}) \begin{bmatrix} \dot{\mathcal{X}} \\ \mu \end{bmatrix} = f(\mathcal{X}, \mathcal{U}, w), \qquad C(\mathcal{X}(t_0)) = 0,$$

where f and $\mathcal{M}$ lump together the process dynamics described in this section. The control vector is given by $\mathcal{U} = \left[\ddot{r}, \ddot{\delta}, \dot{u}_r, \dot{u}_p\right]^T \in \mathbb{R}^4$ and the state vector is given by $\mathcal{X} = \left[P, \dot{P}, e_1, e_2, e_3, \omega_1, \omega_2, \omega_3, r, \dot{r}, \delta, \dot{\delta}, u_r, u_p\right]^T \in \mathbb{R}^{24}$.

B. Measurement Model

The available measurements are coming from the sensors installed on the carousel and on the plane at the KU Leuven and summarized in Table I. Two cameras provide the position of 3 LEDs installed on the plane. The data is passed to the algorithm as the position of the marker u_{M} in the camera plane, given by the pinhole camera model:

Sensor	Measurements	Standard deviation
IMU	Linear acceleration	0.25 m/s^2
IMU	Angular velocity	0.025 rad/s
Cameras	LED position	25 px
Encoder	Tether length	$2.5 \cdot 10^{-3}$ m
Encoder	Carousel angle	$2.5 \cdot 10^{-3}$ rad
Encoder	Control surface angle	$2.5 \cdot 10^{-4}$ rad

TABLE I
AVAILABLE MEASUREMENTS

$$u_{\mathrm{M}} = P_{\mathrm{C}} R_{\mathrm{C}} \left(R p_{\mathrm{M}} + P\right),$$

where p_{M} is the position of the marker in reference frame E, R_{C} is the rotation matrix describing the orientation of the camera and P_{C} is the camera projection matrix. Matrices R_{C} and P_{C}, as well as vector p_M are fixed parameters that have been estimated through camera calibration.

An Inertial Measurement Unit (IMU) is mounted on the plane, which provides measurements for the accelerations and the rotational velocities. While the mounting point of the IMU is assumed to be in the center of mass, the rotation matrix of the IMU with respect to the plane frame R_{IMU} has been identified. The IMU model is thus

$$\begin{aligned} a_{\mathrm{IMU}} &= R_{\mathrm{IMU}}^T \left(\ddot{P} + [0\ 0\ 1]^T g\right), \\ \omega_{\mathrm{IMU}} &= R_{\mathrm{IMU}}^T \omega, \end{aligned}$$

where a_{IMU} are the measured accelerations and ω_{IMU} are the measured rotational velocities.

Additional measurements come from the encoders placed on the rotation axis of the carousel and on the winch, which provide direct measurements of the rotation angle δ and the tether length r. In the following, the outputs of the system will be lumped together in the output function $y(\mathcal{X})$.

C. Constraints

The following control input and state bounds are proposed:

$$\begin{aligned} -20\ \mathrm{rad/s} &\le \dot{u}_k \le 20\ \mathrm{rad/s}, & k &= \{r, p\} \\ -0.5\ \mathrm{m/s^2} &\le \ddot{r} \le 0.5\ \mathrm{m/s^2}, & & \\ -30\ \mathrm{deg/s^2} &\le \ddot{\delta} \le 30\ \mathrm{deg/s^2}, & & \\ -0.3\ \mathrm{rad} &\le u_k \le 0.3\ \mathrm{rad}, & k &= \{r, p\} \\ -1\ \mathrm{m} &\le z & & \end{aligned} \quad (7)$$

In addition to the previous constraints, in order to keep the system in the region where the model assumptions are valid, the following path constraints need to be considered:

$$\begin{aligned} -0.1 \le C_{\mathrm{L}}(\mathcal{X}, w) &\le 1.1, \\ \lambda(\mathcal{X}, w) &\le 0. \end{aligned} \quad (8)$$

Constraint $\lambda \le 0$ is required to keep the tether under tension (model Assumption 1). Constraints on C_{L} are required to prevent the airfoil from stall.

In the following, (7) and (8) are lumped together as the inequality constraint function $h(\mathcal{X}, \mathcal{U}, w) \le 0$.

III. CONTROLLER SYNTHESIS

A. NMPC Formulation

It is proposed here to formulate a receding horizon NMPC scheme using a least squares (LSQ) function penalizing the deviation of the process control inputs and states from the reference trajectories. The NMPC is based on repeatedly ($k = 0, 1, ...$) solving the dynamic optimization problem:

$$\begin{aligned}\mathcal{U}_{\mathrm{c}}(\cdot) = \underset{\mathcal{U}(\cdot),\mathcal{X}(\cdot),\mu(\cdot)}{\operatorname{argmin}} & \frac{1}{2}\left(\|\mathcal{X}-\mathcal{X}_{\mathrm{r}}\|_{P_{\mathrm{LQR}}}\right)_{t=t_0+T_{\mathrm{P}}} \\ & + \frac{1}{2}\int_{t_0}^{t_0+T_{\mathrm{P}}} \left(\|\mathcal{X}-\mathcal{X}_{\mathrm{r}}\|_{Q} + \|\mathcal{U}-\mathcal{U}_{\mathrm{r}}\|_{R}\right) dt, \\ \text{s.t.} \quad & \mathcal{M}(\mathcal{X}) \begin{bmatrix} \dot{\mathcal{X}} \\ \mu \end{bmatrix} = f(\mathcal{X}, \mathcal{U}, w), \\ & \mathcal{X}(t_0) = \hat{\mathcal{X}}(t_0), \quad h(\mathcal{X}, \mathcal{U}, \hat{w}) \leq 0, \end{aligned} \tag{9}$$

where $t_k = k T_{\mathrm{s}}$ and T_{s} is the NMPC sampling time, T_{H} the NMPC prediction horizon, $\mathcal{X}_{\mathrm{r}}$ and $\mathcal{U}_{\mathrm{r}}$ define the state and control reference and Q, R and P_{LQR} are constant positive-definite weighting matrices. Vectors $\hat{\mathcal{X}}(t_k)$ and $\hat{w}(t_k)$ are the process state and wind velocity estimated at time instant t_k by solving problem (10).

Note that the process state estimate must satisfy the consistency condition $C\left(\hat{\mathcal{X}}(t_i)\right) = 0$. However, the consistency conditions are enforced by the state estimator, and therefore need not appear in the NMPC formulation.

The choice of the weighting matrices Q and R is the result of a tuning procedure based on simulations. To compute P_{LQR}, the Riccati equation needs to be solved using the chosen weighting martices Q and R. As the system is modeled by using non-minimal coordinates, invariants are present in the dynamics due to: a) the tether constraint $C(t) = 0$ and b) the orthonormality of the rotation matrix $R^T R = I_3$. Invariants correspond to uncontrollable modes with associated zero eigenvalues and the Riccati equation does not have a solution. To recover the existence of the solution of the Riccati equation, the stabilization of the invariants proposed in [9] has been used.

B. MHE Formulation

It is proposed here to formulate a MHE scheme using a least squares (LSQ) function penalizing the deviation of the process control inputs and outputs from the measurements. The MHE estimate of the state $\hat{\mathcal{X}}(t_k)$ and parameters $\hat{w}(t_k)$ is computed by repeatedly ($i = 0, 1, ...$) solving the following dynamic optimization problem:

$$\begin{aligned}\min_{\mathcal{U}(\cdot),\mathcal{X}(\cdot),\mu(\cdot),w(\cdot)} & \frac{1}{2}\int_{t_0-T_{\mathrm{E}}}^{t_0} \left(\|y(\mathcal{X}) - \bar{y}\|^2_{Q_{\mathrm{E}}} + \|\mathcal{U}-\bar{\mathcal{U}}\|^2_{R_{\mathrm{E}}}\right) dt, \\ \text{s.t.} \quad & \mathcal{M}(\mathcal{X}) \begin{bmatrix} \dot{\mathcal{X}} \\ \mu \end{bmatrix} = f(\mathcal{X}, \mathcal{U}, w), \\ & C(\mathcal{X}(t_0)) = 0, \quad h(\mathcal{X}, \mathcal{U}, w) \leq 0, \end{aligned} \tag{10}$$

where $y(\mathcal{X})$ is the system output function defined in Section II-B, $\bar{y}$ the corresponding set of measurements and Q_E the corresponding covariance matrix. The windspeed w is a parameter that is also estimated by the scheme. The controls computed by the NMPC scheme can differ from those actually applied to the system, due to actuator noise and inaccuracy. The control inputs are thus also included in the MHE formulation as decision variables and their deviation from the inputs provided by the NMPC $\bar{\mathcal{U}}$ is penalized with weights R_E.

C. The Direct Multiple Shooting Method

The system dynamics being unstable, the problems (9) and (10) are best solved using simultaneous approaches [13] such as multiple shooting or collocation. In this paper, a discretization on the uniform time grid $\mathcal{T} = \{t_k \in \mathbb{R},\ k = 1, \ldots, N \mid t_k < t_j,\ \forall k < j\}$ based on the Direct Multiple Shooting method [14] has been used. The discrete-time formulation is thus obtained by independently integrating the system over each time interval $[t_k, t_{k+1}]$ and the path constraints are evaluated on the selected time grid $\mathcal{T}$. The basis functions for the control vector parametrization (CVP) have been chosen piecewise constant. The discretization of both (9) and (10) yields a least-squares NLP, that can be efficiently solved with a Gauss-Newton algorithm. The dimension of the resulting QP is reduced by condensing [15].

D. The Real Time Iterations with Shift

The Real Time Iteration scheme is based on solving only a single full Newton-type iteration per sampling instant. Thanks to the initial value embedding, the computed solution is a good approximation of the exact solution. The needed computations for the RTI scheme reduce to the computation of the sensitivities of the problem and the solution of a single QP. In this context, a clever initialization of the algorithms is crucial to guarantee contractivity of the scheme [5].

Based on the solution at the previous time instant, the initial guess for (9) and (10) is obtained by shifting the state and control vectors $\mathcal{X}$ and $\mathcal{U}$ in time. The last element of each vector needs then to be defined. For the MHE the last controls are set to the ones applied to the system and the last states to the ones predicted by the previous NMPC solution. For the NMPC, the last controls are computed using the discrete-time LQR formulation that yields the weights for the terminal cost, and the states are obtained by forward integration of the dynamics. Note that in the ideal case of tracking a feasible steady-state reference, without perturbations nor noise, the computed initial guess coincides with the exact solution to problems (9) and (10).

The initial value embedding consists in introducing the initial value in the NLP and constraining it to match the estimated state of the system. This makes it possible to simulate the system, compute the sensitivities and thus run most of the computations before the current estimated state $\hat{\mathcal{X}}(t_0)$ becomes available. Once the estimated state is available, the computation of the new controls can be done in a very short time by solving the QP prepared in the previous phase. See [5], [6], [16] for a detailed description of the RTI scheme.

E. ACADO Code Generation

In order to meet the real-time requirements, the code generation tool of ACADO [6], [17] has been used. This

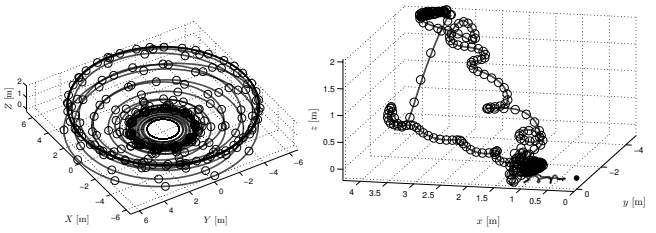


Fig. 1. Aircraft trajectory 3D plot (thick line) with turbulent wind. Left figure (system seen from a fixed point of view): the MHE estimates are shown as circles and the carousel armtip trajectory as a thin line. Right figure (system seen from the carousel arm tip): the MHE estimates are shown as circles and the carousel armtip as a black dot.

tool exports an efficient algorithm based on Direct Multiple Shooting and the RTI scheme. The resulting C code exploits the structure of the specific problem and avoids all irrelevant or redundant computations. The effectiveness of code generation in terms of reduced computational time, has been shown in [6], [18].

F. NMPC and MHE Tuning

The NMPC prediction horizon was set to $T_{\mathrm{H}} = 1\,\mathrm{s}$. The CVP is based on $N = 10$ elements of uniform duration $T_{\mathrm{cvp}}^{\mathrm{NMPC}} = T_{\mathrm{H}}/N$. The system dynamics are discretized over the shooting intervals via an implicit Gauss-Legendre Runge-Kutta integration method of order 2. The NMPC sampling time $T_{\mathrm{s}} = t_i - t_{i-1}$ was chosen as $T_{\mathrm{s}} = T_{\mathrm{cvp}}$. Matrix Q was chosen diagonal, with $\mathrm{diag}\{Q\} = [\,10^{-3}\mathbf{1}_6,\ 10^{-2}\mathbf{1}_{18}]$, where $\mathbf{1}_n$ is a row vector of dimension n, filled with ones. The remaining weights in (9) were chosen as $\mathrm{diag}\{R\} = 10^{-2}\mathbf{1}_4$ and P_{LQR} as the solution to the Riccati equation computed with the chosen weights Q and R. Note that the units of the weights are defined consistently with the variables they correspond to, so as to yield a dimensionless cost.

The chosen MHE estimation horizon was set to $T_{\mathrm{E}} = 1\,\mathrm{s}$. The CVP is based on $N = 10$ elements of uniform duration $T_{\mathrm{cvp}}^{\mathrm{MHE}} = T_{\mathrm{E}}/N$. Matrix Q_E was chosen so as to match the variance of the measurement noise, given in Table I. Based on the same variance, Gaussian noise has been added to all measurements in the proposed simulations.

IV. Start and Landing Strategy

For a tether length $r = 0$ the system is in a singular configuration and the proposed model is not valid. In practice such a configuration is undesirable and the airfoil can be docked to a support at $r \neq 0$.

At very short tether lengths, the system is open loop stable. The control strategy can thus consist in reeling out the tether until a minimal length is reached. By keeping the system in the open loop stable region, MPC and MHE can be warm started. After this phase of initialization, the control algorithms can safely control the process. A similar strategy can be used for landing: the controller needs to bring the system into the open loop stable region and, from there, the tether can be reeled in until the airfoil docks to the carousel.

In this paper it is proposed to track a static reference trajectory, obtained by computing the equilibrium for given height $z = z_r$, tether length $r = r_r$, rotation speed $\dot{\delta} = \dot{\delta}_r$ and

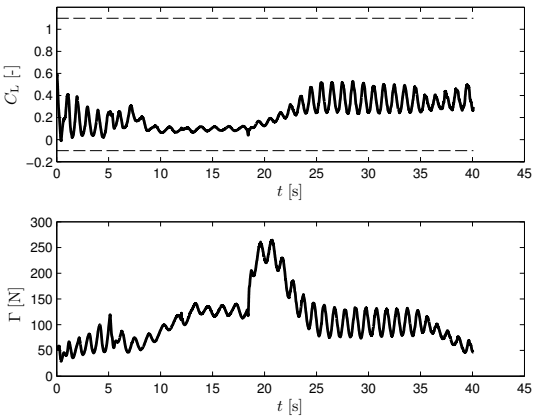


Fig. 2. Lift coefficient C_{L} and tether tension Γ for the given trajectory. The path constraints on those variables are never active.

Time	z_r [m]	r_r [m]	$\dot{\delta}_r$ [rad/s]
$5 \leq t < 11$	0	1.2	2π
$11 \leq t < 23$	2	6.0	1.5π
$23 \leq t < 35$	0	1.2	2π

TABLE II
Reference trajectory for the NMPC.

no wind ($w = 0$). The NMPC and MHE optimization problems being nonconvex, convergence guarantees hold only for initial conditions beeing sufficiently close to the provided reference. The wind being turbulent and the system close to the ground, the best startup strategy consists in designing a trajectory of increasing height and tether length that robustly satisfies the constraints $h(\mathcal{X}, \mathcal{U}, w)$. The computation of such a trajectory involves the solution of a robust optimization problem and is the subject of ongoing research at the KU Leuven.

V. Simulation Results

In this Section, the simulation results obtained for the model proposed in Section II and the control algorithm proposed in Section III are presented. The model parameters are relative to the small scale setup at KU Leuven and are reported in [10]. The proposed scenario considers a turbulent wind, displayed in Fig. 3 (solid line). After 12 s an abrupt change in the wind speed and direction is introduced. At every timestep t_k a static reference, reported in Table II, is provided.

In the first 5 s the tether is reeled out to $r = 1.2$ m. After this phase, the control scheme starts to control the plane by keeping it in the stable region. After 11 s, the reference is changed and the controller elongates the tether and steers the airfoil to an altitude of $z = 2$ m. In the rest of the simulation, the airfoil is controlled back to the stable initial configuration where the tether can be reeled in. The proposed procedure is reversible and the controller is able to safely bring the airfoil to landing.

The trajectory obtained for the given scenario is displayed in Fig. 1 as a thick line, together with the state estimates in circles. It can be seen that in the initial and final part of the trajectory, the airfoil is close to the armtip and no estimate

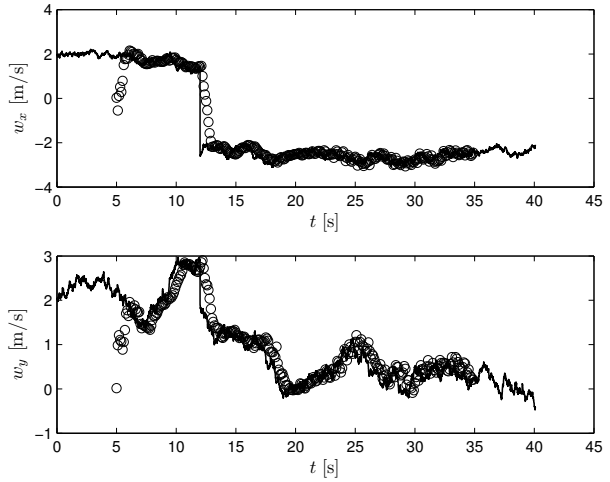


Fig. 3. Real wind profile (x and y components) in continuous line and wind speed estimated by the MHE (x and y components) in circles.

is shown, as the system is in the open-loop stable region and doesn't need any feedback control.

The lift coefficient and the tether tension are displayed in Fig. 2. Note that the proposed path constraints are never active for the proposed scenario. The proposed scheme is able to adequately control the system in the proposed scenario, while respecting the state and control bounds.

The x and y components of the wind speed are introduced as parameters to be estimated by the MHE scheme. Their estimates are displayed in Fig. 3 in circles. Though no direct measurement of the wind speed is available, it can be seen that the proposed MHE scheme provides a good estimate to both wind speed and direction. The introduction of adequate wind models in the MHE scheme is subject of ongoing research at the KU leuven.

The simulations were run on a 2.8 GHz CPU and the computational times are displayed in Fig. 4. The computational times are consistently below $T_s = 100$ ms, allowing for a real-time implementation. While the simulations show the effectiveness of the control scheme, a thorough study on its robustness would require an extensive simulation and experimental campaign which is out of the scope of this paper.

VI. Conclusion & Further developments

This paper has proposed a control strategy for the launch and retrieval of tethered airfoils in perturbed wind conditions. A highly descriptive 6-DOF control model has been used for the control and estimation schemes.

The estimation and the control problem have been tackled using MHE and NMPC respectively. To meet the real-time requirements, automatic code generation of efficient algorithms has been used.

The proposed scheme has been able to control the system in the presence of turbulent wind with abrupt changes without any direct wind speed measurement. The tether has been extended to 6 m and the flying height has reached 2 m.

Future work will focus on the computation of robust trajectories for launching and landing. The control of the

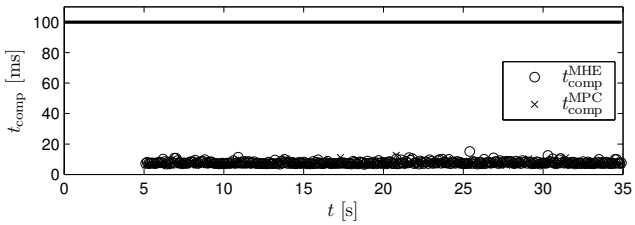


Fig. 4. Computational times t_{comp} for the MPC (crosses) and MHE (circles) scheme. The sampling time $T_s = 100$ ms is represented by a thick line.

complete power production cycle (i.e.: startup, power extraction and landing) under various wind conditions is subject of ongoing research at the KU Leuven. A small scale setup is currently being built to test the proposed algorithms in open air experiments.

References

[1] J. Laks, L. Pao, and A. Wright, "Control of Wind Turbines: Past, Present, and Future," in *American Control Conference*, pp. 2096–2103, 2009.

[2] E. A. Bossanyi, "Further Load Reductions with Individual Pitch Control," *Wind Energy*, vol. 8, pp. 481–485, 2005.

[3] M. Loyd, "Crosswind Kite Power," *Journal of Energy*, vol. 4, pp. 106–111, July 1980.

[4] S. Gros, M. Zanon, and M. Diehl, "Orbit Control for a Power Generating Airfoil Based on Nonlinear MPC," in *American Control Conference*, 2012. (submitted).

[5] M. Diehl, H. Bock, J. Schlöder, R. Findeisen, Z. Nagy, and F. Allgöwer, "Real-time optimization and Nonlinear Model Predictive Control of Processes governed by differential-algebraic equations," *Journal of Process Control*, vol. 12, no. 4, pp. 577–585, 2002.

[6] B. Houska, H. Ferreau, and M. Diehl, "An Auto-Generated Real-Time Iteration Algorithm for Nonlinear MPC in the Microsecond Range," *Automatica*, vol. 47, no. 10, pp. 2279–2285, 2011.

[7] A. Ilzhoefer, B. Houska, and M. Diehl, "Nonlinear MPC of kites under varying wind conditions for a new class of large scale wind power generators," *International Journal of Robust and Nonlinear Control*, vol. 17, no. 17, pp. 1590–1599, 2007.

[8] H. Ferreau, B. Houska, K. Geebelen, and M. Diehl, "Real-time control of a kite-carousel using an auto-generated nonlinear MPC algorithm," in *Proceedings of the IFAC World Congress*, 2011.

[9] S. Gros, M. Zanon, M. Vukov, and M. Diehl, "Nonlinear MPC and MHE for Mechanical Multi-Body Systems with Application to Fast Tethered Airplanes," in *Proceedings of the 4th IFAC Nonlinear Model Predictive Control Conference, Noordwijkerhout, The Netherlands*, 2012.

[10] S. Gros, H. Ahmad, K. Geebelen, and M. Diehl, "In-flight estimation of the aerodynamic roll damping and trim angle for a tethered aircraft based on multiple-shooting," in *System Identification Conference*, 2012.

[11] Pamadi, *Performance, Stability, Dynamics, and Control of Airplanes*. American Institute of Aeronautics and Astronautics, Inc., 2003.

[12] M. V. Cook, *Flight Dynamics Principles*. Elsevier Science, 2007.

[13] L. Biegler, "An overview of simultaneous strategies for dynamic optimization," *Chemical Engineering and Processing*, vol. 46, pp. 1043–1053, 2007.

[14] H. Bock and K. Plitt, "A multiple shooting algorithm for direct solution of optimal control problems," in *Proceedings 9th IFAC World Congress Budapest*, pp. 243–247, Pergamon Press, 1984.

[15] D. Leineweber, I. Bauer, A. Schäfer, H. Bock, and J. Schlöder, "An Efficient Multiple Shooting Based Reduced SQP Strategy for Large-Scale Dynamic Process Optimization (Parts I and II)," *Computers and Chemical Engineering*, vol. 27, pp. 157–174, 2003.

[16] M. Diehl, H. Bock, and J. Schlöder, "A real-time iteration scheme for nonlinear optimization in optimal feedback control," *SIAM Journal on Control and Optimization*, vol. 43, no. 5, pp. 1714–1736, 2005.

[17] H. Ferreau, T. Kraus, M. Vukov, W. Saeys, and M. Diehl, "High-speed moving horizon estimation based on automatic code generation," in *Proceedings of the 51th IEEE Conference on Decision and Control (CDC 2012), Hawaii*, 2012.

[18] H. Ferreau, *Model Predictive Control Algorithms for Applications with Millisecond Timescales*. PhD thesis, K.U. Leuven, 2011.